IEEE Access
Multidisciplinary ⋮ Rapid Review ⋮ Open Access Journal

Received 18 August 2025, accepted 1 September 2025,
date of publication 5 September 2025, date of current version 12 September 2025.

Digital Object Identifier 10.1109/ACCESS.2025.3606439

RESEARCH ARTICLE

Toward Passive Sensing Large Crowds Through User-Generated Electromagnetic Activity

DENNIS JOOSENS, (Graduate Student Member, IEEE), ABDIL KAYA, (Graduate Student Member, IEEE), RUBEN NIETVELT, (Graduate Student Member, IEEE), MAARTEN WEYN, (Member, IEEE), AND RAFAEL BERKVENS, (Member, IEEE)
IDLab—imec, Faculty of Applied Engineering, University of Antwerp, 2000 Antwerp, Belgium

Corresponding author: Dennis Joosens (dennis.joosens@uantwerpen.be)

This work was supported in part by the Research Foundation—Flanders [Fonds Wetenschappelijk Onderzoek (FWO)] Passive Environment Sensing through Signals of Opportunity (PESSO) Project under Grant G018522N. The work of Abdil Kaya was supported by FWO under Grant 1S99720N.

ABSTRACT The emerging field of Joint Communication and Sensing (JCAS) will have a substantial impact on future wireless communication systems and how people interact with them. The investigation of sensing large crowds with these communication systems still lacks thorough exploration. Current studies are generally based on small-scale experiments with few participants. However, these studies are not representative in comparison to large crowds. By passively sensing an environment, it is possible to link the captured electromagnetic (EM) activity within that area to the crowd size without applying any demodulation or decoding of packets and preserving privacy. Measurements were conducted in an exclusive area at a large music festival, using ten Software-Defined Radios (SDRs) to capture EM wave energy across several Wi-Fi and LTE bands. The collected data were compared to a validation data set. The study shows that the short-time Fourier transform (STFT) and the magnitude extraction technique are two viable techniques to apply to the captured data sets. Additionally, the correlations found between the validation data set and the LTE data sets are significantly stronger than those in the Wi-Fi data sets. This indicates that further research is needed on specific frequency band selection, advanced digital signal processing methods and scalable data-capturing strategies.

INDEX TERMS Crowd size, electromagnetic wave energy, JCAS, LTE, magnitude extraction, passive sensing, STFT, Wi-Fi.

I. INTRODUCTION

The nascent field of Joint Communication and Sensing (JCAS) will become an important part of the Sixth Generation of Wireless Technologies (6G) and even beyond. The idea of transforming wireless networks into sensors seems unattainable, yet it will have a tremendous impact on how people interact with these networks. Additionally, efficient spectrum usage is becoming significantly important. Wild et al. claim that with the ongoing evolution of 5G and 6G, bandwidths in the order of 1 GHz or more are expected, which can enable high-resolution sensing capabilities [1]. Although many of these new applications are aimed at industrial or environmental use, objects and persons will have the leading role in this field. When examining the currently investigated methods of sensing crowds in environments, it is found that it can be achieved using low-cost Received Signal Strength Indication (RSSI) based methods. These methods are straightforward to implement but are prone to multipath effects that influence the accuracy of these systems [2], [3]. Another common method is Channel State Information (CSI), which can be used for crowd counting at a small-scale, device-free activity and gesture recognition using Wi-Fi and LTE [4], [5], [6], [7], [8]. A final method, which is

The associate editor coordinating the review of this manuscript and approving it for publication was Fan-Hsun Tseng.

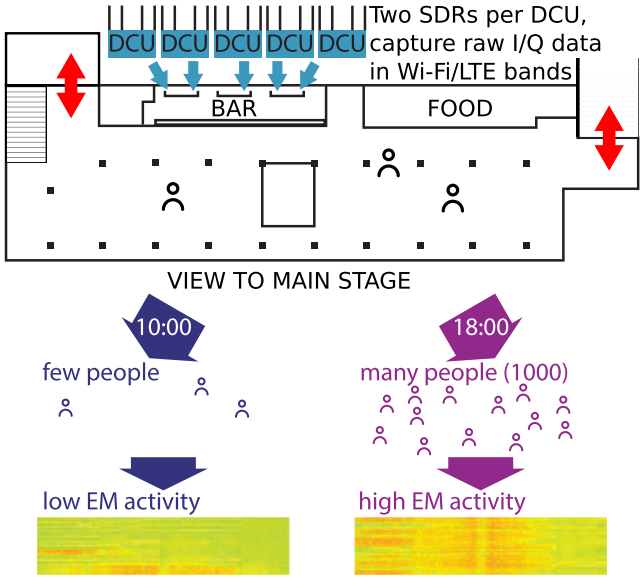

FIGURE 1. Top view of the measurement area where five DCUs are deployed. The hypothesis states that it is feasible to link crowd sizes through the proxy of the EM activity found in Wi-Fi and LTE bands.

being thoroughly investigated, is the use of Passive Wi-Fi Radar (PWR). This method typically uses Wi-Fi access points and Software-Defined Radios (SDRs), which need two synchronised receiver channels. A surveillance channel receives the reflecting signals, while the reference channel has a direct path link to the transmitted signal [6], [9]. This technique typically works well in small-scale experiments. In summary, these methods strongly focus on activity recognition, localisation, tracking, and presence detection [10]. Upon examining the methods currently under investigation in the field of JCAS, it becomes apparent that little to no research is conducted on passive crowd size sensing. This presents an opportunity for exploratory investigation. By defining passive crowd size sensing as the detection and collection of the crowds' generated electromagnetic (EM) activity of any transceiver that they carry. This implies that persons can have any active communication link to a third-party system, but do not have any active connection to the presented measurement setup. This means that this deployed sensing system is external to other possible available communication systems. It is important to note that there is no prior knowledge of the number of transmitters in the vicinity. Subsequently, it is needed to sense in a privacy-aware fashion. This means that no demodulation and decoding of packets is applied. To validate the obtained data, a device-free or non-invasive sensing system is used. The system senses or detects persons without relying on persons being equipped with any transceiver [3], [11]. The hypothesis, which is depicted in Fig. 1, states that it is achievable to link the number of people in an area through the use of generated EM activity. Whereas low activity indicates few people on the premises, high activity means many people are in the area of interest.

In Section II, the systems applied in the measurement environment are discussed, including the data set used for validation. Furthermore, the applied signal processing techniques to the gathered data sets are explained. Additionally, the scaling of the Power Spectral Density (PSD) functions over time is investigated. Eventually, the standards and guidelines regarding electromagnetic field exposure are briefly touched upon. Thereafter, the results are shown, which are extensively discussed in Section III. Finally, conclusions are drawn regarding the work and a look at future research is given in Section IV.

II. METHODOLOGY

The measurements are conducted at an exclusive area of the Tomorrowland music festival in Boom, Belgium. The festival took place for two weekends in July 2023 and hosted about 200 000 attendees per weekend. The measurement setups were placed in the business-to-business (B2B) environment. This area spanned about 1500 m^2 and is located between two other exclusive environments, which are part of a three-storey construction with a view of the festival's main stage. To sense the environment, i.e. measure the EM wave energy, five Data Capture Units (DCUs) are placed behind the bar of the storey at a height of three metres. Each DCU contains two Ettus Research Universal Software Radio Peripherals (USRP) B210 SDR devices onboard, which are connected to omnidirectional dipole antennas. Each USRP has an instantaneous bandwidth of 56 MHz and a frequency receiving range from 70 MHz up to 6 GHz. Per DCU, an Intel NUC is responsible for the sampling process and storing the generated complex baseband data. If a sample of a Wi-Fi channel of 20 MHz is recorded continuously for one hour, this will result in 288 GB of data without having any data loss. This would be unmaintainable in terms of data storage and post-processing. Therefore, 40 random samples per hour are recorded throughout the entire weekend, where each sample lasts one second. Eventually, a total of 2560 In-phase and Quadrature (I/Q) samples during 64 hours were obtained per captured channel for weekend one. A random sampling method is a type of probability sampling that is straightforward to implement and has the benefit of reducing bias while maintaining representativeness.

The setup is configured in a way that three DCUs capture two standard non-overlapping Wi-Fi channels in the 2.4 GHz band. DCU 2 and 4 were configured similarly for comparison and redundancy, whereas DCU 3 recorded samples in a more commonly used data type. DCU 2 and DCU 4 save data in the complex short 16 data type, whereas DCU 3 records data in the complex float 32 data type. However, no data loss occurs when using the complex short 16 data type. This is because the Analogue-to-Digital Converter (ADC) in the USRP B210 has a 12-bit resolution. The data is converted to a larger data type by the USRP Hardware Driver (UHD) upon request of the specific application. The use of a smaller data type does affect the scale of the data. In particular, the scale or dynamic range will be altered by 96.33 dB. This value is calculated

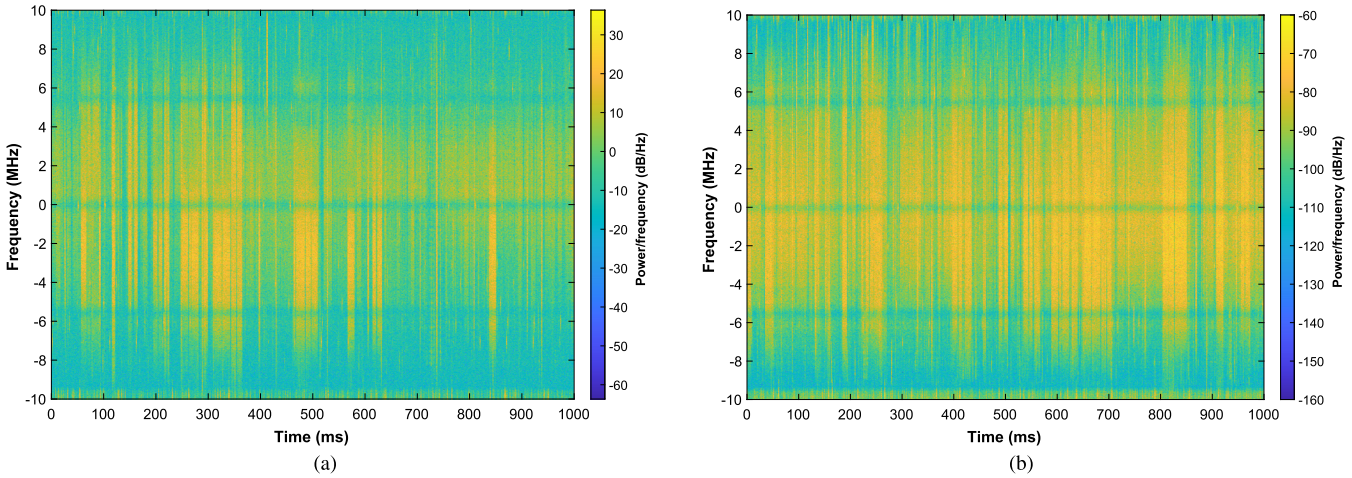

FIGURE 2. Comparison of a random complex short 16 sample (a) and a random complex float 32 sample (b) with matched scaling. The Power Spectral Density of the sample is shown on a scale of 100 dB/Hz. It is discernible that there is a scaling offset between the samples.

TABLE 1. Overview of the configured centre frequencies, captured bandwidths and used data types per DCU.

	F_c (MHz)	Bandwidth (MHz)	Data type (complex)
DCU 2 Wi-Fi CH 1	2412	20	int 16
DCU 2 Wi-Fi CH 11	2462	20	int 16
DCU 3 Wi-Fi CH 1	2412	20	float 32
DCU 3 Wi-Fi CH 11	2462	20	float 32
DCU 4 Wi-Fi CH 1	2412	20	int 16
DCU 4 Wi-Fi CH 11	2462	20	int 16
DCU 1 LTE BAND 1	816	10	int 16
DCU 1 LTE BAND 2	1837.5	25	int 16
DCU 5 LTE BAND 3	2162.5	25	int 16
DCU 5 LTE BAND 4	2680	20	int 16

as follows,

$$\Delta_{difference} = 20\log_{10}(2^n), \tag{1}$$

where n is the number of bits in difference per I-or Q-component. In this case, n is equal to 16. To clarify this further, the spectrograms of two random data samples of both data types with a corrected scale are depicted in Fig. 2. A more extensive clarification of these spectrograms can be found in Section II-E. DCU 1 and 5 were configured to capture specific LTE downlink Frequency-Division Duplex (FDD) channels. Hereby, the focus was on the LTE bands used by the three major Telecommunications Service Providers (TSPs) in Belgium [12]. The rationale behind using legacy Wi-Fi and LTE is their omnipresence, along with attainable and similar bandwidth. This can be observed in Table 1. Wi-Fi 5 GHz and 5G cellular bands could have been another choice to investigate. However, newer technologies generally use higher bandwidths, which translates into more data. To make a similar comparison for these newer technologies, more expensive SDRs and additional data storage are needed to capture these EM waves. Additionally, data processing will be more computationally

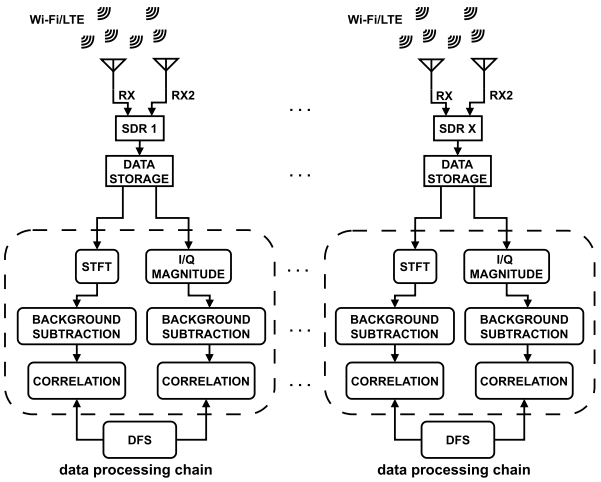

FIGURE 3. Overview of the data capturing process and the post-processing chain, which is applied in the same way for each data set.

intensive. Table 1 depicts the used centre frequencies F_c, bandwidths, and used data types for storage.

A. VALIDATION DATA SET

The Device-Free Sensing (DFS) system was deployed to the area of interest, serving as a ground truth reference system. This system is based on a Wireless Sensor Network (WSN) and uses the DASH7 Alliance Protocol (D7AP). The network consists of several nodes that are placed at the edge of the measurement area. In this setup, 27 transceivers were used. The nodes send and receive RSSI values to one another as a vector. These transmissions, and therefore the RSSI values, are affected by the human bodies within the area of interest. Eventually, all these RSSI vectors are collected and processed by a gateway that computes a mean attenuation value. This system is a proper validation system as it is thoroughly deployed and tested by Denis et al. [11], [13], [14].

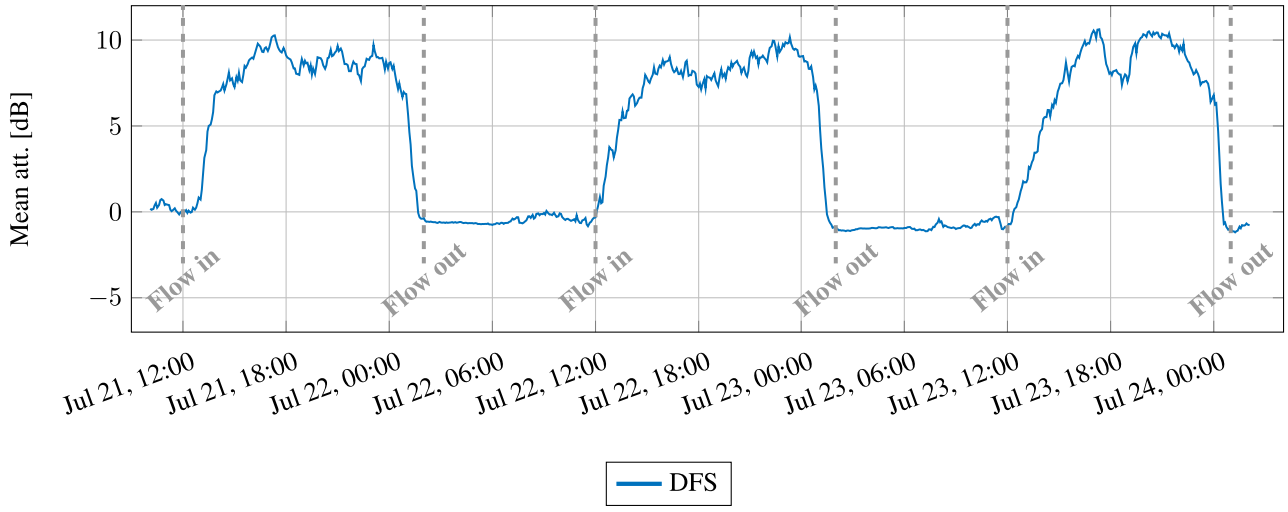

FIGURE 4. A depiction of the attenuation of the Device-Free Sensing data during weekend one. The graph contains six markers that indicate the opening and closing of each day of the festival.

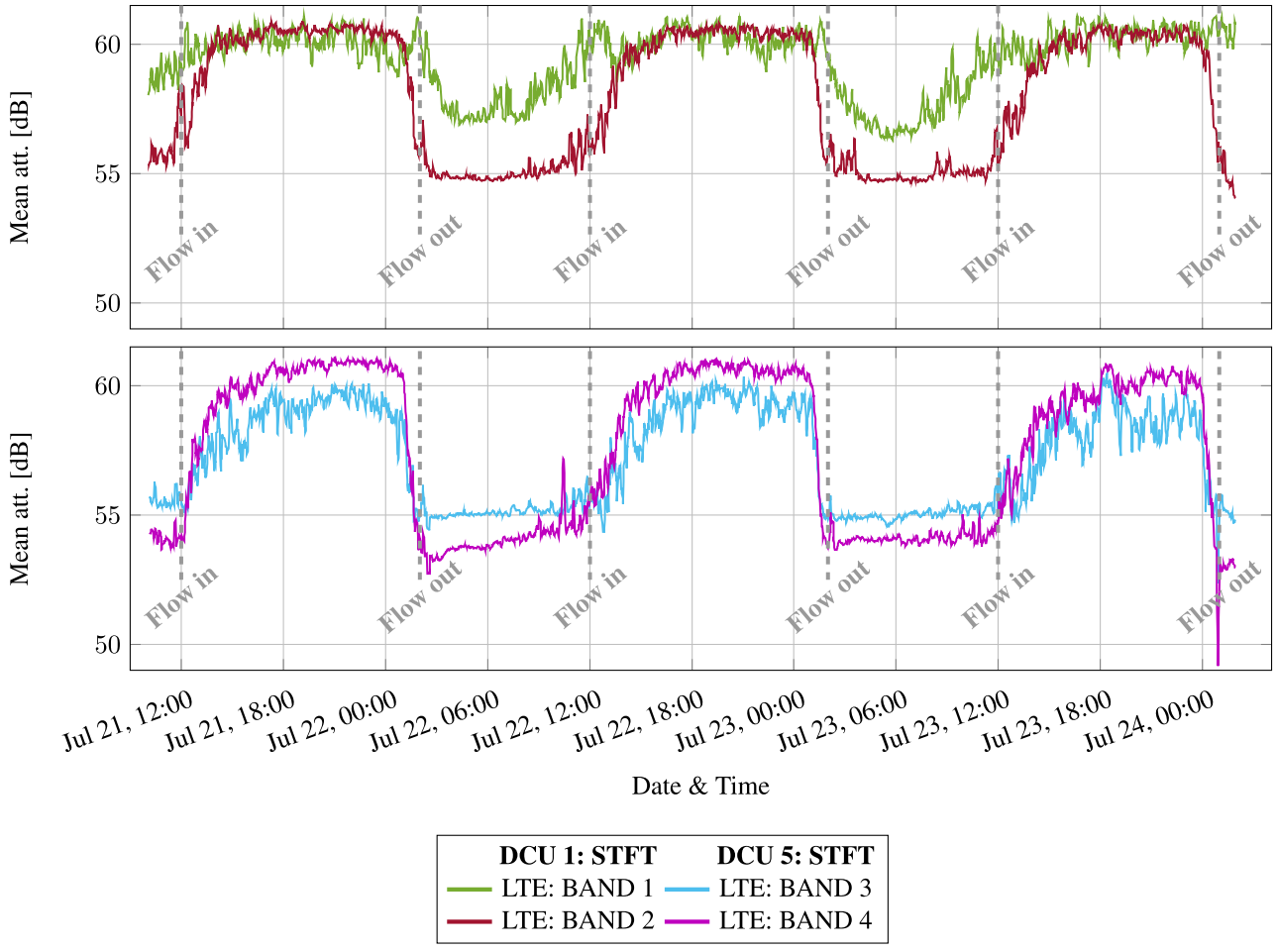

FIGURE 5. The two figures show the activity within four different LTE channels when the STFT is applied. For each graph, six markers are found, which indicate the opening and the closing per day of the festival. It can be seen that, overall, the fluctuations do not differ significantly between the LTE channels.

B. SHORT-TIME FOURIER TRANSFORM

The short-time Fourier transform (STFT) is one of the many time-frequency analysis techniques available for non-stationary signals [15]. The technique segments time-domain signals into several frames. These frames are subsequently multiplied by a sliding window function acting

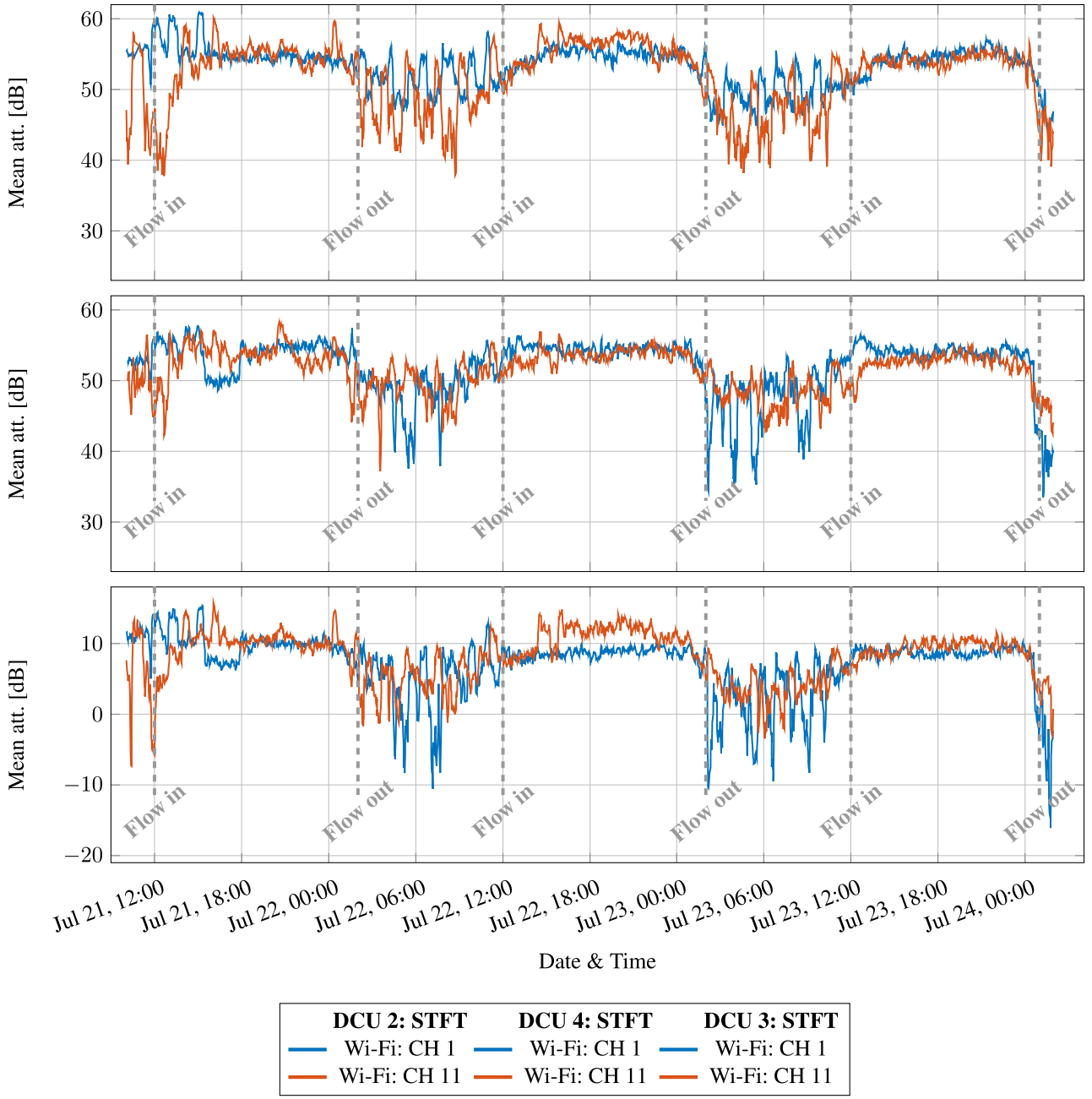

FIGURE 6. **The three figures depict the EM wave activity over three consecutive days during weekend one of the festival, when the STFT is applied. Wi-Fi channel 1 is shown in blue and Wi-Fi channel 11 in red for each DCU. For each graph, six markers are found, which indicate the opening and the closing per day of the festival. It can be seen that fluctuations differ significantly between these time slots per day, per Wi-Fi channel and DCU.**

as a filter. Consequently, the discrete Fourier transform (DFT) is applied to each frame. By using this DFT operation, combined with a sliding window, a better view of the spectral content changes of the signal is obtained. The discrete STFT is defined as:

$$S_{[m,n]} = \sum_{k=0}^{L-1} x[k]w[k-m]e^{-j2\pi k\frac{n}{L}}, \tag{2}$$

where $S_{[m,n]}$ is a function of time and frequency while m is the frame index, n is the frequency bin index and k is the time index. L is the window length or frame length. $w[k]$ is the specified window function of L-points multiplied with the discrete time signal $x[k]$. Lastly, multiplication by a complex sinusoid with a frequency defined by $\frac{n}{L}$, which is part of the DFT process. Eventually, an averaged energy value of the obtained matrix is calculated,

$$\overline{X_{[m,n]}} = \frac{1}{N}\sum_{n=0}^{N-1} \left|S_{[m,n]}\right|. \tag{3}$$

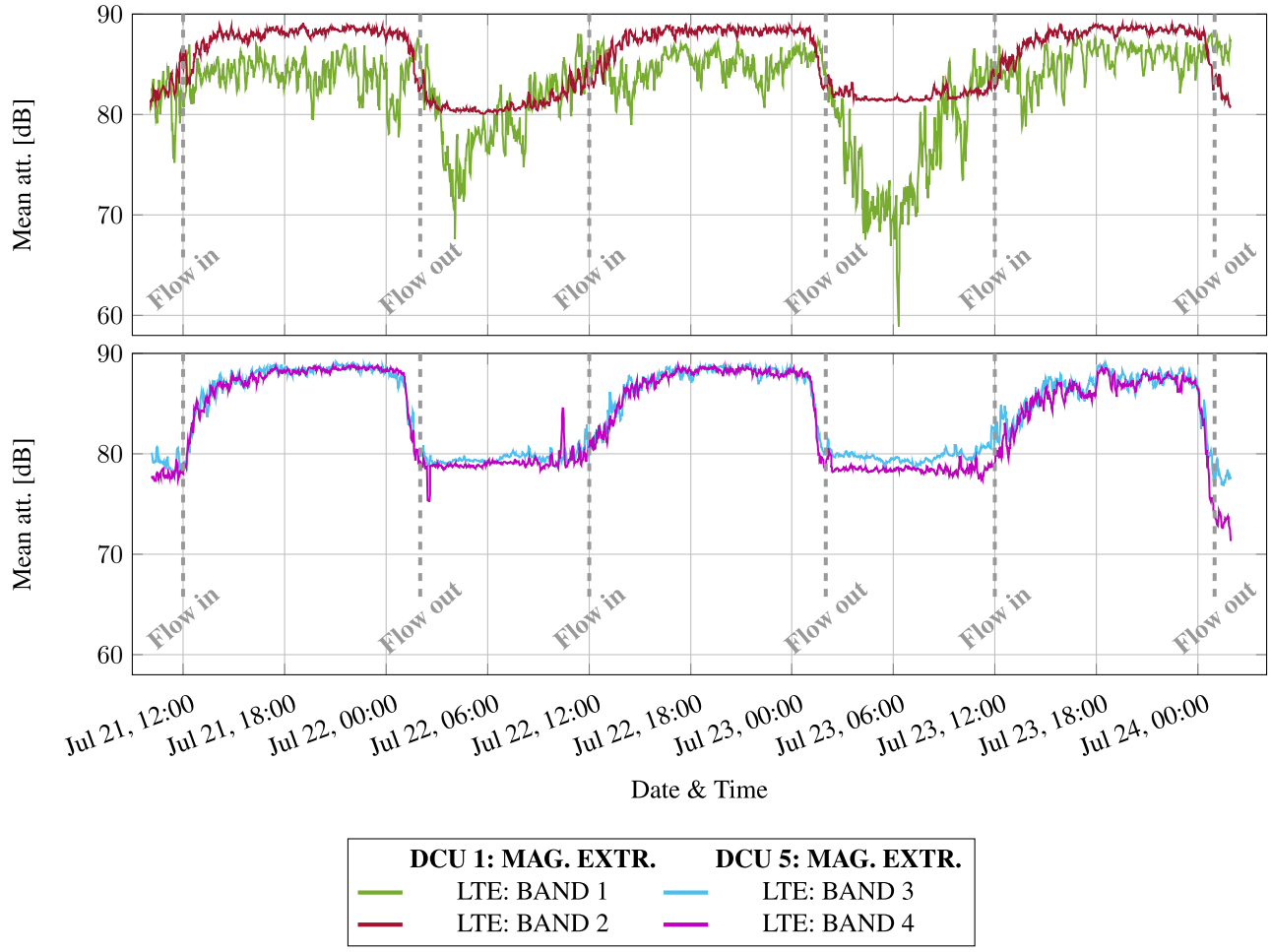

FIGURE 7. The two figures show the activity when the magnitude extraction method is applied within four different LTE channels. For each graph, six markers are found, which indicate the opening and the closing per day of the festival. It can be seen that, overall, the fluctuations do not differ significantly between the LTE channels.

Finally, a moving average over five samples is applied, which smooths and decreases the effect of possible high peaks or low valleys. Eventually, this smoothed data is converted to a logarithmic scale to obtain the Power Spectral Density. This can be expressed as:

$$PSD_{S[m,n]} = 10\log_{10}(\frac{1}{5}\sum_{i=k}^{k+4}\overline{X_{[m,n]_i}}). \tag{4}$$

The spectral and temporal components that are gained can be visualised in two or three dimensions. The third component is the magnitude variation of the EM waves over time, interpreted as activity or no activity. These activity markers are seen as the signal strengths of the samples over time. Due to the uncertainty principle of the Fourier transform, it is impossible to have good time and frequency resolution simultaneously [16]. This means that the achieved results are always a trade-off. However, at this moment, the interest lies more in the change of EM activity over time rather than specific frequency changes. Consequently, selecting a smaller window should gain a better time resolution. Nevertheless, to decrease computation time, the same parameters as used in the initial work are applied [17]. A Hamming window is initiated with 0% overlap between segments and setting the number of DFT points and window size to 16 384.

C. BACKGROUND SUBTRACTION

By applying background subtraction to the Wi-Fi and LTE data sets, a fair view is attained of what is happening in the spectrograms of the samples. This is achieved by subtracting nocturnal data recordings from the effective data. In this way, the effect of static EM wave transceivers in the environment is reduced. The result, i.e. the background-subtracted mean attenuation per channel of the Wi-Fi and LTE data sets, is visualised in Fig. 5 and Fig. 6. The effect of the technique is that the fluctuations within the data sets become more visible. The background data sets are based on 440 samples recorded at night, i.e. the period after one festival day ends and before the next begins. First, an STFT operation is applied to each background sample. The STFT of the background samples returns a matrix in the time-frequency domain filled with

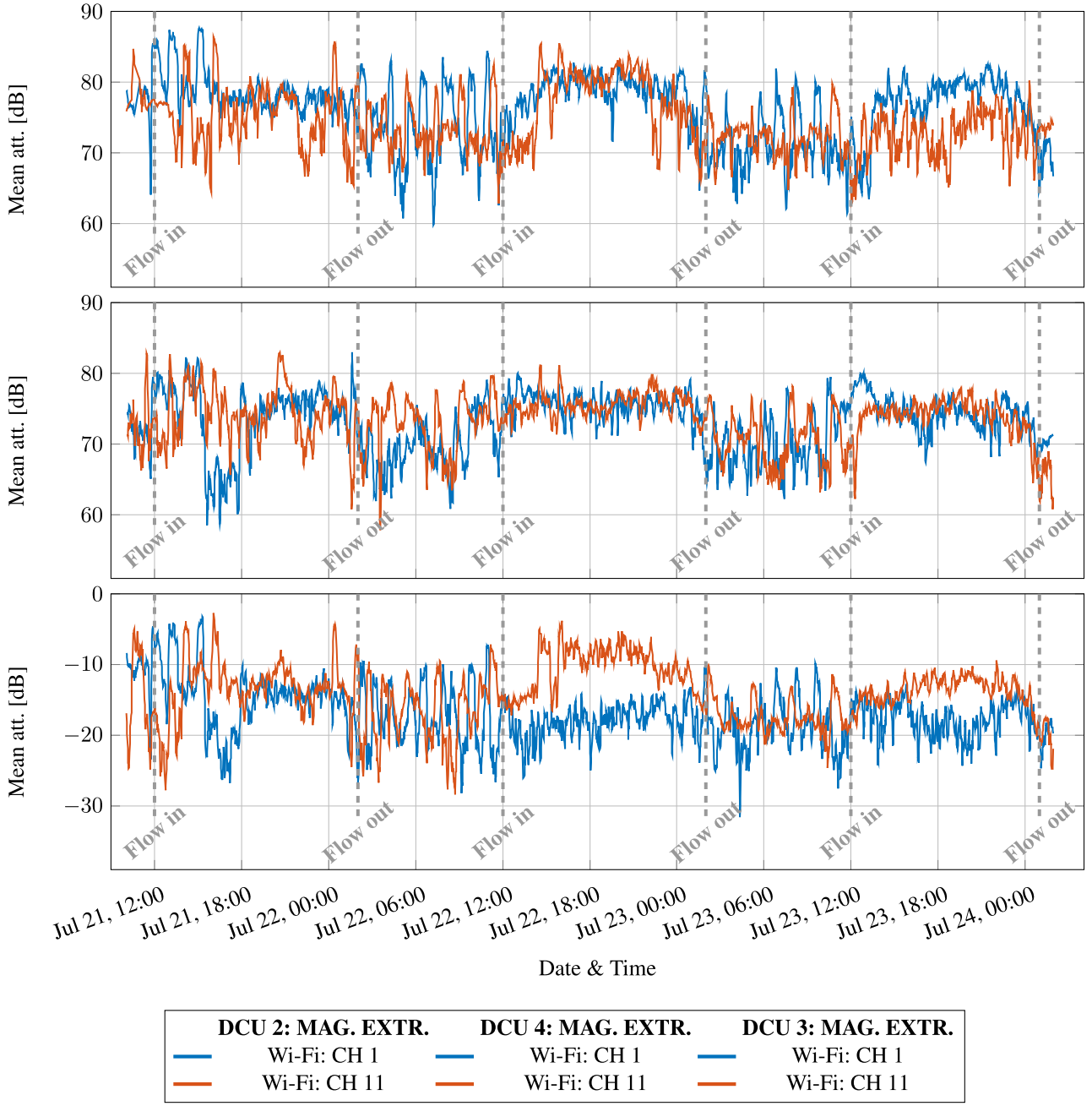

FIGURE 8. The three figures depict the activity when the magnitude extraction method is applied over three consecutive days during the first weekend of the festival. Wi-Fi channel 1 is shown in blue and Wi-Fi channel 11 in red for each DCU. For each graph, six markers are found, which indicate the opening and the closing per day of the festival. It can be seen that fluctuations differ significantly between these time slots per day, per Wi-Fi channel and DCU.

complex numbers:

$$S_{bg} \in \mathbb{C}^{t \times f}. \tag{5}$$

Notice that the same process is applied as stated in Equation (2) and (3). Subsequently, the average of this matrix is obtained as follows:

$$\overline{S_{bg}} = \sum_{i}^{B} \frac{S^{(i)}}{B}, \tag{6}$$

with B being the number of samples used to calculate the background and i being the index of each sample in the set of samples. The same STFT settings as in Section II-B are applied to the background data samples.

Thereafter, the mean attenuation of the I/Q data samples with background subtraction, i.e. $a_{\neg bg}$ is calculated as:

$$a_{\neg bg} = \sum\nolimits_{t,f} \frac{(S - \overline{S_{bg}})}{N}. \tag{7}$$

This will gain the EM activity per Wi-Fi channel. In Equation (7), S is the STFT of the I/Q data samples in which these complex samples are converted to magnitude values, while N is the number of elements in S. Aside from background subtraction and sample-averaging, no other noise filtering methods are applied.

D. MAGNITUDE EXTRACTION

A more exploratory, but less computationally intensive method that was investigated is raw I/Q-pair magnitude extraction. The magnitude of an I/Q sample is, in essence, the representation of the voltage amplitude of the captured wave at a specific moment in time. The data sets that were recorded contain complex-valued baseband signals. To obtain the instantaneous magnitude of a particular Wi-Fi or LTE I/Q sample, i.e. a phasor, the root of the sum of the squared quadrature components is taken. Subsequently, this operation is applied to all the samples within one recording and eventually averaged,

$$P_{d[n]} = \frac{1}{N}\sum_{i=1}^{N}\sqrt{I_i^2 + Q_i^2}. \tag{8}$$

The power of the samples is calculated by taking the logarithmic magnitude squared,

$$P_{d[n](dB)} = 10\log_{10}(P_{d[n]}^2). \tag{9}$$

Finally, a moving average operation is applied as shown in Equation (4). A complete overview of the data capturing process and post-processing chain can be found in Fig. 3. The results for weekend one for the DFS system are found in Fig. 4, whereas the results for the STFT process are found in Fig. 5 and Fig. 6. The outcome of the magnitude extraction technique is found in Fig. 7 and Fig. 8. Subsequently, the comparison between these data sets and the DFS data set is clarified by calculating the Pearson and Kendall correlations. These results are found in Table 2 and Table 3.

E. POWER SPECTRAL DENSITY SCALING

When calculating the STFT of a data sample, a third dimension is gained. This is the energy over time and frequency, or power over each frequency bin. Since measuring the correct amount of energy over time is crucial for passive crowd size sensing, it is essential to interpret these measured values correctly. As a preliminary point, it is important to know what the lowest value in a sample is. This is achieved by finding the noise power or Johnson-Nyquist noise of a sample, which forms the start of defining the noise floor.

A theoretical approach to finding the noise power can gain a better insight into the values that are shown in Fig. 2 (a) and Fig. 2 (b), and eventually it will make more sense of the outcome of the entire data set. The theoretical thermal noise power or noise power per unit bandwidth is defined as,

$$P_N = k\,T_0\,B. \tag{10}$$

In this equation, k is the Boltzmann constant, i.e. $k \approx 1.38 \cdot 10^{-23}$ J/K, T_0 is the environmental temperature in Kelvin, i.e., 300 K, and B which defines the noise-equivalent bandwidth [18], [19]. This thermal noise power equals -204 dB/Hz, which is the amount of noise power in a bandwidth of 1 Hz measured at the environmental temperature [18]. By adding 30 dB, the noise floor of the sample can be found, i.e. -174 dBm/Hz. To be more accurate, this calculation needs adaptation. In general, higher bandwidths are used in the conducted experiments, i.e. 10 MHz to 25 MHz; therefore, the theoretical noise power will be higher. For a bandwidth of 20 MHz it can be found as follows,

$$\begin{aligned} P_{N,20\,\text{MHz}} &= k\,T_0\,B \\ &= 1.38 \cdot 10^{-23}\,\text{J/K} \cdot 300\,\text{K} \cdot 20 \cdot 10^6\,\text{Hz} \\ &= -203.98\,\text{dB/Hz} \;+\; 10 \cdot \log_{10}(20 \cdot 10^6\,\text{Hz}) \\ &= -130.82\,\text{dB}/20\,\text{MHz}. \end{aligned} \tag{11}$$

Additionally, the Noise Figure (NF) of the hardware needs to be taken into account, which can be found by taking the noise factor, F and expressing it in decibels:

$$\begin{aligned} NF_{dB} &= 10\,log_{10}(F) \\ &= 10\,log_{10}(\frac{S_i}{N_i} - \frac{S_o}{N_o}). \end{aligned} \tag{12}$$

where $\frac{S_i}{N_i}$ is the ratio of input signal power to input noise power, and where $\frac{S_o}{N_o}$ is the ratio of output signal power to output noise power. The NF essentially is the amount of noise a hardware system, i.e. mixers, amplifiers, filters, etc., adds to an incoming signal. Although the NF is not explicitly defined for the SDRs used in this study, as the SDR can span a wide range of frequencies. It is found that the NF will be smaller than 8 dB. For convenience, 8 dB is used in the calculation,

$$\begin{aligned} N_{\text{system}} &= N_{20\,\text{MHz}} + NF \\ &= -130.82\,\text{dB} + 8\,\text{dB} \\ &= -122.82\,\text{dB}/20\,\text{MHz}. \end{aligned} \tag{13}$$

This gains a theoretical noise floor of -122.82 dB for the current sample. When adding the dynamic range of the ADC to this noise power, the sample value ranges from -122.82 dB to -26.49 dB. Note that the PSD in MATLAB is calculated on a windowed segment and not over 1 Hz. For the current setting in this study, the length is 16 384, corresponding to 1220.7 Hz, at which the noise power is calculated, which will gain,

$$\begin{aligned} P_{N,1220.7\,\text{Hz}} &= k \cdot T_0 \cdot B \\ &= 1.38 \cdot 10^{-23}\,\text{J/K} \cdot 300\,\text{K} \cdot 1220.7\,\text{Hz} \\ &= -203.98\,\text{dB/Hz} + 30.87\,\text{dB/Hz} \\ &= -173.11\,\text{dB}/1220.7\,\text{Hz}. \end{aligned} \tag{14}$$

However, this value is not used as a minimum value because the bandwidth was initially 20 MHz. When investigating the minimum value measured of the sample displayed in Fig. 2,

TABLE 2. Summary of the correlations and confidence intervals of each DCU per channel of each Wi-Fi and LTE data set to the DFS validation data set after the STFT and background subtraction operation is applied.

STFT	DCU 2 DFS - Wi-Fi		DCU 3 DFS - Wi-Fi		DCU 4 DFS - Wi-Fi		DCU 1 DFS - LTE		DCU 5 DFS - LTE	
	CH 1	CH 11	CH 1	CH 11	CH 1	CH 11	BAND 1	BAND 2	BAND 3	BAND 4
Pearson's r	0.404	0.634	0.303	0.628	0.513	0.627	0.594	0.935	0.839	0.944
95% CI_{upper}	0.436	0.657	0.338	0.651	0.541	0.650	0.619	0.940	0.850	0.948
95% CI_{lower}	0.371	0.611	0.267	0.604	0.484	0.603	0.568	0.930	0.827	0.940
Kendall's τ	0.411	0.448	0.311	0.500	0.357	0.463	0.406	0.625	0.569	0.618

TABLE 3. Summary of the correlations and confidence intervals of each DCU per channel of each Wi-Fi and LTE data set to the DFS validation data set after the magnitude operation and background subtraction is applied.

MAG. EXTR.	DCU 2 DFS - Wi-Fi		DCU 3 DFS - Wi-Fi		DCU 4 DFS - Wi-Fi		DCU 1 DFS - LTE		DCU 5 DFS - LTE	
	CH 1	CH 11	CH 1	CH 11	CH 1	CH 11	BAND 1	BAND 2	BAND 3	BAND 4
Pearson's r	0.273	0.406	-0.013	0.362	0.227	0.305	0.597	0.938	0.867	0.930
95% CI_{upper}	0.308	0.438	0.023	0.395	0.264	0.340	0.622	0.943	0.876	0.935
95% CI_{lower}	0.236	0.373	-0.052	0.328	0.190	0.270	0.572	0.934	0.857	0.925
Kendall's τ	0.332	0.347	0.112	0.372	0.209	0.281	0.395	0.633	0.596	0.620

it is found that the current scale has an offset. Still, it does not affect the comparison made between the two samples. It is noted that the theoretical noise power is close to the measured minimum. The difference between the measured values is 118.21 dB, which is an extensive range. It can be found that the values below −130.82 dB can be interpreted as noise. As a final note, the SDRs used in this work are by default not calibrated to a known power reference, which affects the measured signal values. This means that these devices are not precise RF field-probing devices. This also indicates that the measured noise power of each device and even each channel per SDR can vary. Therefore, the measured PSD values within this work should be interpreted as relative indicators rather than absolute power levels from the environment.

F. ELECTROMAGNETIC FIELD EXPOSURE STANDARDS AND GUIDELINES

Within this study, a lot of data is collected, and it can be interesting to investigate the potential effects of these radio waves on crowds. Organisations such as the International Commission of Non-Ionising Radiation Protection (ICNIRP) and the Institute of Electrical and Electronics Engineers (IEEE) define guidelines and set exposure limits to commonly used frequency bands [20], [21]. The primary concern of these organisations is the effect of thermal heating, i.e., tissue heating and whole-body heating, caused by Electromagnetic Fields (EMF). These organisations define a baseline to avoid adverse health effects and maintain public safety. ICNIRP has set whole-body reference levels, which are 50 W m^{-2} for occupational public exposure while defining 10 W m^{-2} for general public exposure, for frequencies up to 10 GHz which are averaged over 30 minutes, over the whole-body space, which causes a body core temperature rise of 1 °C. In a recent study, ICNIRP identifies several gaps in the literature, one of which is to clarify the relation between whole-body exposure and core temperature rise from 100 kHz to 300 GHz, as a function of exposure duration and combined EMF exposures [22]. Recently, a systematic review was conducted by Ramirez-Vasquez et al., synthesising data from 86 studies published between 1998 and 2023 [23]. The overall consensus is that the levels measured during these studies are far below the conservative levels of ICNIRP. In another study conducted by Vecsei et al., personal exposure measurements were executed at a large outdoor festival where a high-end measurement of 0.2 W m^{-2} was found [24]. Therefore, it is safe to assume that the ambient RF signals that are monitored passively in this experiment are not causing harm to the crowd.

III. RESULTS AND DISCUSSION

A strong correlation is required between an EM data set and the validation data set to link the crowd size in a specific area to the EM activity. As mentioned in Section II-A for validation, the results achieved by the DFS system are used. The obtained mean attenuation of the festival's first Friday, Saturday and Sunday can be found at the top of Fig. 4. This graph shows the measured mean attenuation on a scale between -1.28 dB and 10.90 dB. It is also noteworthy that in Fig. 6 and in Fig. 8, the mean attenuation range of DCU 3 shows an entirely different scale compared to DCU 2 and DCU 4. This occurs when a different data type is used, which consequently alters the measured relative amplitude. Nevertheless, this does not affect the absolute delta of the results as stated in Section II. The correlations between the DFS data set and the different EM data sets are statistically significant ($p < 0.05$) except for the negative value in Table 3. Table 2 depicts the correlations found when an STFT process and background subtraction are applied as described in Section II-B and Section II-C. Whereas Table 3 depicts the correlations when magnitude extraction and background subtraction are applied, which is described in Section II-C and II-D. Remarkably, the correlations in general of the LTE data sets are notably higher than those of the Wi-Fi data sets. Furthermore, the LTE data sets show more subtle

changes and, therefore, a relatively flat response. In contrast, the Wi-Fi data sets fluctuate heavily during the day and even more during the night; this may clarify the lower correlations. The correlations are low, moderate to even high for the Wi-Fi data sets, whereas the LTE data sets show robust correlations. Additionally, the tables depict the 95% confidence intervals for both techniques. It is found that when the correlations are substantial, these values are close to the Pearson correlation. The trends of day and night are also more difficult to distinguish for the Wi-Fi data sets compared to the LTE data sets. This can be seen even better with the six markers indicating the opening and closing of the festival per day as shown on Fig. 5, 6, 7 and 8. When looking closely at the regions of these markers in Fig. 6 and Fig. 8, it is shown that the fluctuations differ significantly between signals on similar and different Wi-Fi channels in the same time slot of a day. When looking deeper into Fig. 5 and Fig. 7, these fluctuations are relatively small. Furthermore, the activity also varies considerably per Wi-Fi channel compared to a different DCU. Another significant difference compared with the venue setup in the previous work is that complimentary Wi-Fi was offered to the festival attendees, which can adversely affect the measured activity. This might indicate that the current Wi-Fi channels are not heavily used. It is plausible that, besides the 2.4 GHz band, the 5 GHz band was used more extensively to cope with the amount of data traffic generated by the users. Furthermore, investigating channel 1 and channel 11, only represents 48.8% of the total 2.4 GHz band. In general, the Kendall coefficients are lower than the calculated Pearson values. This indicates that severe opposite fluctuations are happening in the data sets when ranked. Fluctuations in the LTE data sets are in the range of 7 dB to 12 dB. For the Wi-Fi data sets, this difference is higher, ranging from 24 dB to 35 dB, which implies that high fluctuations are more noticeable in the Wi-Fi data sets and less represented in the LTE data sets. This also contributes to the low correlations found for the Wi-Fi data sets. The correlations of the magnitude extraction method appear to deteriorate the Wi-Fi correlations but slightly improve the LTE correlations. The latter method reduces complexity and requires less computation time, and therefore, it seems a plausible candidate for simplifying data analysis.

On the other hand, a deep investigation of how these systems work can be beneficial in understanding the behaviour of these technologies. Wi-Fi is a Wireless Local Area Network (WLAN) technology, whereas LTE is a Wireless Wide Area Network (WWAN). Unquestionably, both technologies are affected by external factors outside of the area of interest. However, this is an insurmountable consequence of wireless technologies, as well as the way the measurement setup is built. For the LTE data sets, only the LTE downlink energy is examined, which gives good results; however, looking into LTE uplink energy can provide a better local view of what is happening in the wireless channel near the area of interest.

IV. CONCLUSION

In this work, two methods are investigated to link the number of people in a crowded environment through the proxy of EM activity while expanding the number of samples taken and the technologies to use. The first method that was applied is the STFT with background subtraction, which shows the frequency changes over time. In contrast, the magnitude extraction method applies an operation on raw I/Q data that returns the magnitude of a phasor at a specific point in time.

In general, it is found that the STFT method does not necessarily lead to better results when compared to the magnitude extraction method for the Wi-Fi data set, but the opposite is true for the LTE data set. The latter method has a substantial adverse effect on the Wi-Fi data sets, whereas for the LTE data set, it slightly improves the results. The correlations between the DFS system and the energy found in the LTE bands are significantly stronger than those in the Wi-Fi bands. Subsequently, the correlations are better in channel 11 compared to channel 1. This indicates that channel 11 is used more often than channel 1.

These results and observations indicate more paths to explore, whereas the presented methods are the starting point. Expanding the measurement setup and the sampling bands more strategically can be one of the options. Furthermore, taking more samples per hour or working towards a real-time measurement setup is another track to investigate. However, both methods will require more storage capacity.

Furthermore, there is a need for a comprehensive study of digital signal processing techniques that can be applied to the EM data sets. These techniques could eventually gain better results regarding correlations and, thereby, in people counts. Currently, the average attenuation value of a full sample is calculated. These values might include noise, which can be perceived as effective EM energy. Applying specific filtering techniques or data-slicing techniques can significantly reduce or even eliminate these effects.

REFERENCES

[1] T. Wild, V. Braun, and H. Viswanathan, "Joint design of communication and sensing for beyond 5G and 6G systems," *IEEE Access*, vol. 9, pp. 30845–30857, 2021.

[2] W. Xue, W. Qiu, X. Hua, and K. Yu, "Improved Wi-Fi RSSI measurement for indoor localization," *IEEE Sensors J.*, vol. 17, no. 7, pp. 2224–2230, Apr. 2017.

[3] J. Wang, Q. Gao, M. Pan, and Y. Fang, "Device-free wireless sensing: Challenges, opportunities, and applications," *IEEE Netw.*, vol. 32, no. 2, pp. 132–137, Mar. 2018.

[4] T. Li, C. Shi, P. Li, and P. Chen, "A novel gesture recognition system based on CSI extracted from a smartphone with nexmon firmware," *Sensors*, vol. 21, no. 1, p. 222, Dec. 2020.

[5] S. Liu, Y. Zhao, F. Xue, B. Chen, and X. Chen, "DeepCount: Crowd counting with WiFi via deep learning," 2019, *arXiv:1903.05316*.

[6] M. J. Bocus, W. Li, J. Paulavicius, R. McConville, R. Santos-Rodriguez, K. Chetty, and R. Piechocki, "Translation resilient opportunistic WiFi sensing," in *Proc. 25th Int. Conf. Pattern Recognit. (ICPR)*, Jan. 2021, pp. 5627–5633.

[7] J. A. Zhang, M. L. Rahman, K. Wu, X. Huang, Y. J. Guo, S. Chen, and J. Yuan, "Enabling joint communication and radar sensing in mobile networks—A survey," *IEEE Commun. Surveys Tuts.*, vol. 24, no. 1, pp. 306–345, 1st Quart., 2022.

[8] Z. Wu, P. Ji, M. Ma, W. Zhuang, Z. Li, J. Cui, and Z. Wang, "Crowd counting based on WiFi channel state information and transfer learning," *J. Comput. Commun.*, vol. 10, no. 6, pp. 22–36, 2022.
[9] W. Li, R. J. Piechocki, K. Woodbridge, C. Tang, and K. Chetty, "Passive WiFi radar for human sensing using a stand-alone access point," *IEEE Trans. Geosci. Remote Sens.*, vol. 59, no. 3, pp. 1986–1998, Mar. 2021.
[10] S. Savazzi, S. Sigg, M. Nicoli, V. Rampa, S. Kianoush, and U. Spagnolini, "Wireless sensing for device-free recognition of human motion," in *Radar for Indoor Monitoring: Detection, Classification, and Assessment*. Boca Raton, FL, USA: CRC Press, Oct. 2017, pp. 337–363, doi: 10.1201/9781315155340-14.
[11] S. Denis, B. Bellekens, M. Weyn, and R. Berkvens, "Sensing thousands of visitors using radio frequency," *IEEE Syst. J.*, vol. 15, no. 4, pp. 5090–5093, Dec. 2021.
[12] Belgian Institute for Postal Services and Telecommunications (BIPT). (Jun. 2010). *Frequency Plan*. Accessed: Jul. 17, 2025. [Online]. Available: https://www.bipt.be/consumers/frequency-plan
[13] S. Denis, A. Kaya, R. Berkvens, and M. Weyn, "Device-free localization and identification using sub-GHz passive radio mapping," *Appl. Sci.*, vol. 10, no. 18, p. 6183, 2020.
[14] S. Denis, B. Bellekens, A. Kaya, R. Berkvens, and M. Weyn, "Large-scale crowd analysis through the use of passive radio sensing networks," *Sensors*, vol. 20, no. 9, p. 2624, May 2020.
[15] R. Marks, *Handbook of Fourier Analysis & Its Applications*. London, U.K.: Oxford Univ. Press, 2009.
[16] V. Chen and H. Ling, *Time-Frequency Transforms for Radar Imaging and Signal Analysis* (Artech House Radar Library). Norwood, MA, USA: Artech House, 2002.
[17] D. Joosens, A. Kaya, M. Weyn, and R. Berkvens, "Crowd size estimation with passive electromagnetic sensing," in *Proc. IEEE Int. Conf. Commun. Workshops (ICC Workshops)*, May 2023, pp. 672–678.
[18] A. Molisch, *Wireless Communications: From Fundamentals to Beyond 5G*, 3rd ed., Hoboken, NJ, USA: Wiley, 2022.
[19] Y. J. Morton, F. Van Diggelen, J. J. Spilker Jr., and B. W. Parkinson, *Position, Navigation, and Timing Technologies in the 21st Century: Integrated Satellite Navigation, Sensor Systems, and Civil Applications*. Hoboken, NJ, USA: Wiley, 2020.
[20] *IEEE Standard for Safety Levels With Respect to Human Exposure to Electric, Magnetic, and Electromagnetic Fields, 0 Hz to 300 GHz*, IEEE Standard C95.1-2019, 2019, pp. 1–312.
[21] ICNIRP, "Guidelines for limiting exposure to electromagnetic fields (100 KHz to 300 GHz)," *Health Phys.*, vol. 118, no. 5, pp. 483–524, 2020.
[22] International Commission on Non-Ionizing Radiation Protection (ICNIRP), "Gaps in knowledge relevant to the 'ICNIRP guidelines for limiting exposure to time-varying electric, magnetic and electromagnetic fields (100 KHz to 300 GHz),'" *Health Phys.*, vol. 128, no. 2, pp. 190–202, 2025.
[23] R. Ramirez-Vazquez, I. Escobar, E. Arribas, and G. A. E. Vandenbosch, "Systematic review of exposure studies to radiofrequency electromagnetic fields: Spot measurements and mixed methodologies," *Appl. Sci.*, vol. 14, no. 23, p. 11161, Nov. 2024.
[24] Z. Vecsei, Z. Szilágyi, and G. Thuróczy, "Radiofrequency personal exposimetry during outdoor entertainment of young adults: A case study," *Radiat. Protection Dosimetry*, vol. 199, nos. 8–9, pp. 865–871, May 2023.

DENNIS JOOSENS (Graduate Student Member, IEEE) received the master's degree in applied engineering from the University of Antwerp, Belgium, in 2018. He is a Doctoral Researcher with the University of Antwerp. His Ph.D. research with the IDLab—imec Research Group, focused on passive sensing crowds leveraging personal wireless technologies and passive radar sensing.

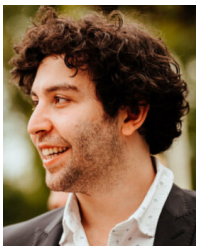

ABDIL KAYA (Graduate Student Member, IEEE) received the master's degree in applied engineering: electronics-ICT and the Ph.D. degree in radio frequency-based device-free crowd sensing from the University of Antwerp, Belgium, in 2018 and 2024, respectively. During his research, he has published several publications on this topic, along with the publication of a large-scale data set.

RUBEN NIETVELT (Graduate Student Member, IEEE) received the M.Sc. degree in applied engineering: electronics-ICT from the University of Antwerp, Belgium, in 2023, where he is currently pursuing the Ph.D. degree with the IDLab—imec Research Group. His research interests include integrated sensing and communication and the use of wireless technologies for localization.

MAARTEN WEYN (Member, IEEE) received the Ph.D. degree in computer science on the topic of opportunistic seamless localization from the University of Antwerp, Antwerp, Belgium, in 2011. He is currently a Full Professor and the Vice-Rector of Research and Impact with the University of Antwerp. He teaches wireless communication systems. His research with IDLab—imec focuses on ultra-low power sensor communication, embedded systems, sub-1 GHz communication, sensor processing, and localization. He has co-founded spin-offs Aloxy, CrowdScan, IoSa, and AtSharp, contributed to 1OK and Viloc, and a maker on the Canvas Program Team Scheire.

RAFAEL BERKVENS (Member, IEEE) received the master's degree in applied engineering: electronics-ICT and the Ph.D. degree in indoor location information quantification from the University of Antwerp, Belgium, in 2012 and 2017, respectively. Currently, he is an Assistant Professor with IDLab—imec, Department of Electronic, Information and Communication Technology, Faculty of Applied Engineering, University of Antwerp. His research focuses on perception through ambient wireless communication, integrated sensing and communication, and intelligent transportation systems. He is a member of the IEEE Communications Society. He chairs the subject group of communication, teaches several networking courses, and coordinates part of the master's project.